

## Local vertical compressive stress in the crane runway beam web

Lukasz Polus<sup>1</sup>, Marcin Chybiński<sup>2</sup>, Zdzisław Kurzawa<sup>3</sup>

<sup>1</sup> Institute of Building Engineering; Faculty of Civil and Transport Engineering;  
Poznan University of Technology; Piotrowo 5, 60-965 Poznań, Poland;  
lukasz.polus@put.poznan.pl  0000-0002-1005-9239

<sup>2</sup> Institute of Building Engineering; Faculty of Civil and Transport Engineering;  
Poznan University of Technology; Piotrowo 5, 60-965 Poznań, Poland;  
marcin.chybinski@put.poznan.pl  0000-0003-2539-7764

<sup>3</sup> The President Stanislaw Wojciechowski Calisia University;  
Nowy Świat 4, 62-800 Kalisz, Poland  
zd.kurzawa@gmail.com

**Abstract:** In this paper, the authors analysed several variants of connections between a block rail (60 mm × 60 mm) and a crane runway beam (IKS 800-6). They compared local vertical compressive stress in the crane runway beam web, calculated using an analytical approach and numerical simulations. In the case of the continuous block rail rigidly fixed to the beam flange, satisfactory convergence was obtained. For the remaining types of connections the results based on the analytical method were different from the results of the numerical simulations. The difference resulted from the fact that the analytical method did not take into account the crane rail joint. Furthermore, the impact of the elastomeric bearing pad on the local stress value was taken into account in a simplified manner in the analytical method by increasing the effective length by approximately 30%. The local vertical compressive stress in the crane runway beam web was significantly affected by the connection between the rail and the crane runway beam, the crane rail joint type, the use of the elastomeric bearing pad, the length of the elastomeric bearing pad, and the crane rail wear.

**Keywords:** crane runway beam, local stress, crane rail, steel structures

### 1. Introduction

Crane actions are separated into vertical and horizontal in the standard [1]. They induce dynamic and cyclic loadings [2]. In the designing process, the dynamic effects of the lifting of the weight, the crane movement and the trolley movement are taken into account using dynamic factors [3]. Vertical actions are caused by the self-weight of the crane and the hoist load. Horizontal crane actions are caused by acceleration or deceleration, skewing or other

dynamic effects. The vertical loads of the crane runway beams result in global stress because of the bending around the  $y$  axis and torsion. The horizontal loads result in global stress because of the bending around the  $z$  axis and torsion. The vertical loads cause not only global stress but also local stress. The local vertical compressive stress is generated in the web of the crane runway beams. The global stress is superposed with the local stress in the beam web using Eq. (1) [4]–[6]:

$$\left(\frac{\sigma_{x,Ed}}{f_y/\gamma_{M0}}\right)^2 + \left(\frac{\sigma_{z,Ed}}{f_y/\gamma_{M0}}\right)^2 - \left(\frac{\sigma_{x,Ed}}{f_y/\gamma_{M0}}\right)\left(\frac{\sigma_{z,Ed}}{f_y/\gamma_{M0}}\right) + 3\left(\frac{\tau_{Ed}}{f_y/\gamma_{M0}}\right)^2 \leq 1.0 \quad (1)$$

where:  $f_y$  – the yield strength,  $\gamma_{M0}$  – the partial factor,  $\sigma_{x,Ed}$  – the design value of the longitudinal stress,  $\sigma_{z,Ed}$  – the design value of the transverse stress,  $\tau_{Ed}$  – the design value of the shear stress.

The local vertical compressive stress in the web  $\sigma_{oz,Ed}$  is used in Eq. (1) as transverse stress. Due to the cyclic nature of the crane actions, it also is necessary to carry out fatigue assessments, taking into account the local vertical compressive stress in the case of crane runway beams [7]–[9].

The local vertical compressive stress in the web  $\sigma_{oz,Ed}$  is calculated using the following equation from the EN 1993-6 standard [10]:

$$\sigma_{oz,Ed} = \frac{F_{z,Ed}}{l_{eff}t_w} \quad (2)$$

where:  $F_{z,Ed}$  – the design value of the wheel load,  $t_w$  – the web thickness,  $l_{eff}$  – the effective loaded length.

The value of the local vertical compressive stress depends on the distance below the underside of the top flange:

$$\sigma_{oz,Ed} = \frac{F_{z,Ed}}{l_{eff}t_w} \left(1 - \frac{2z}{h_w}\right) \quad (3)$$

where:  $z$  – the distance below the underside of the top flange,  $h_w$  – the overall depth of the web.

The real distribution of the local vertical compressive stress in the web is presented in Fig. 1a. In the standard [10] a constant stress distribution was assumed over the effective length (Fig. 1b).

The effective loaded length may be determined using the following equations from the EN 1993-6 standard [10]:

- for a crane rail rigidly fixed to the beam flange:

$$l_{eff} = 3.25 [l_{rf}/t_w]^{1/3} \quad (4)$$

- for a crane rail not rigidly fixed to the beam flange:

$$l_{eff} = 3.25 \left[ (I_r + I_{f,eff}) / t_w \right]^{1/3} \quad (5)$$

- for a crane rail mounted on a suitable resilient elastomeric bearing pad at least 6 mm thick:

$$l_{eff} = 4.25 \left[ (I_r + I_{f,eff}) / t_w \right]^{1/3} \quad (6)$$

where:  $I_{rf}$  – the second moment of area about its horizontal axis, of the combined cross-section comprising the rail and the beam flange with an effective width,  $I_r$  – the second moment of area about its horizontal axis of the rail,  $I_{f,eff}$  – the second moment of area about its horizontal axis of a flange with an effective width.

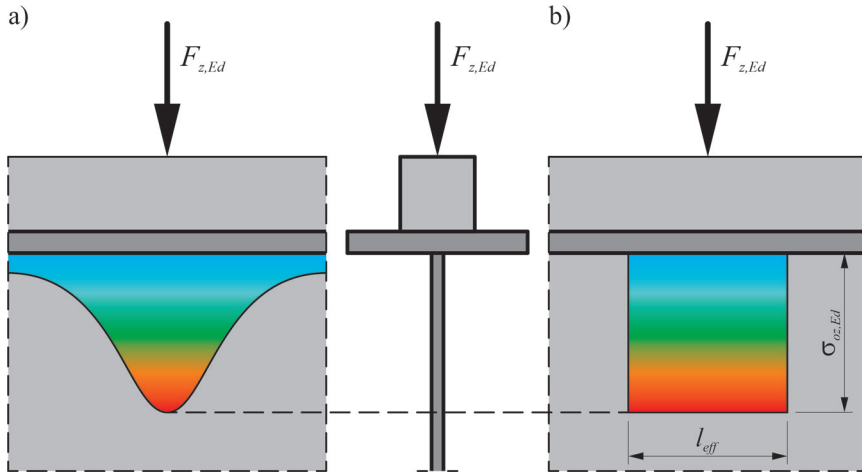


Fig. 1. Local vertical compressive stress in the web: a) real distribution, b) constant stress distribution assumed over the effective length

The effective width of a flange is calculated as [10]:

$$b_{eff} = b_{fr} + h_r + t_f \text{ but } b_{eff} \leq b \quad (7)$$

where:  $b$  – the overall width of the top flange,  $b_{fr}$  – the width of the foot of the rail,  $h_r$  – the height of the rail,  $t_f$  – the flange thickness.

As outlined above, the effective loaded length depends on the type of the connection between a crane rail and a beam flange (rigid or flexible). Furthermore, the effective length may be increased when the elastomeric bearing pad is used under the rail. According to the

EN 1993-6 standard [10], the effective length for a crane rail mounted on a suitable resilient elastomeric bearing pad is 1.3 times higher than the one for a crane rail mounted without the elastic underlay. The elastomeric bearing pad provides for a smoother stress distribution in the beam web [11]–[13]. Mass [14] and Marcinczak [15] observed a significant decrease in the local stress value when the elastic underlay was applied. What is more, the value of the effective length and consequently the value of the local stress depends on the crane rail condition. Kurzawa et al. [16] observed the increase of the local vertical compressive stress in the crane runway beam web resulting from the crane rail wear. According to the EN 1993-6 standard [10] and papers [17]–[19], the wear of a rail should already be taken into account in the design process by reducing the head of the rail by 25%. Moreover, Chybiński et al. [20] demonstrated that the value of the local vertical compressive stress depends on the crane rail type. Rykaluk et al. [21] demonstrated that the value of the local vertical compressive stress depends on the shape of the crane rail splice. Last but not least, in his laboratory tests Kurzawa observed that the deformation of an elastomeric bearing pad subjected to vertical load depends on the friction force between the crane rail and the beam flange [11]. During the operation of the crane rails, oiling may occur on the contact surfaces. Kurzawa investigated the impact of oiling on the deformation of the elastomeric bearing pad. The behaviour of oiled elastomeric bearing pads was compared with that of dry bearing pads. Different elastomeric bearing pad thicknesses and types were taken into account, i.e., neoprene elastomeric bearing pads, polyurethane elastomeric bearing pads with and without steel plates, timber pads saturated under pressure with polyurethane. As a result of these tests Kurzawa obtained bearing stress–relative vertical deformation curves. The relative values of the vertical deformation were obtained by dividing the deformation by the thickness of the pad. Figure 2 presents the curve for the 15 mm neoprene elastomeric bearing pad. The deformation of the oiled elastomeric bearing pads was higher than the one of dry pads. The increase of the deformation due to oiling may have an impact on the stress in the crane rails and in the web of the crane runway beam. For this reason, it should be analysed in future tests.

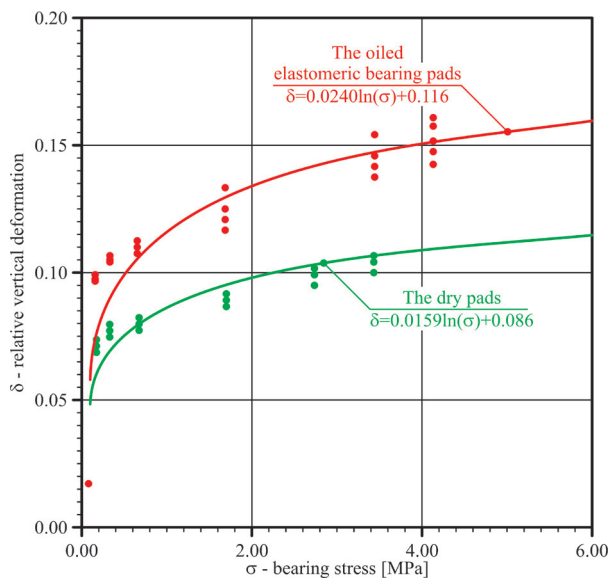


Fig. 2. Bearing stress–relative vertical deformation curves for oiled and dry 15 mm neoprene elastomeric bearing pads [11]

## 2. The aim of the current study

In this study a block rail ( $60\text{ mm} \times 60\text{ mm}$ ) connected with a crane runway beam (IKS 800-6) was analysed in several variants (Figs 3, 4).

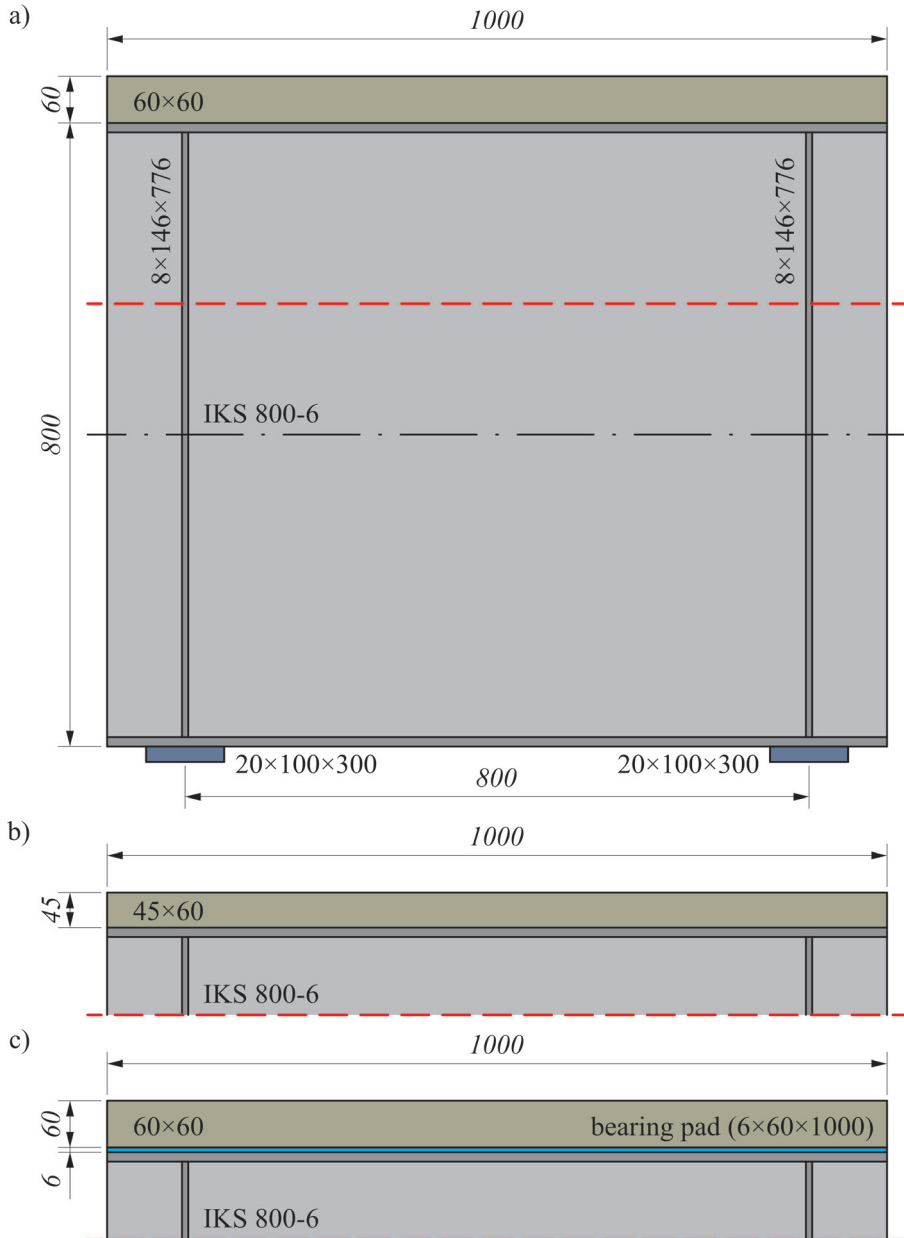


Fig. 3. Variants analysed in this study: a) the block rail rigidly (analysis 1) or flexibly fixed (analysis 3) to the beam flange; b) the reduced block rail rigidly (analysis 2) or flexibly fixed (analysis 4) to the beam flange; c) the block rail mounted on a  $6\text{ mm} \times 60\text{ mm} \times 1000\text{ mm}$  elastomeric bearing pad (analysis 5)

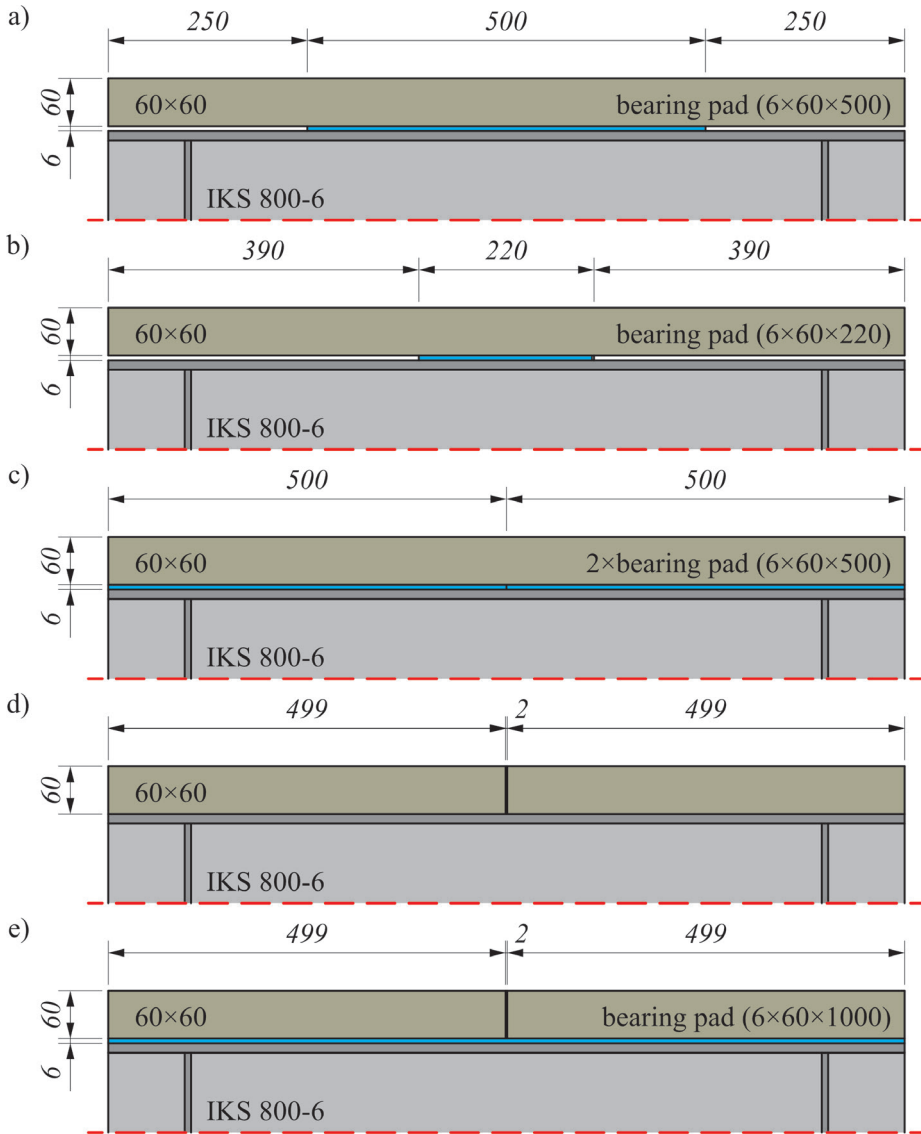


Fig. 4. Variants analysed in this study: a) the block rail mounted on a 6 mm × 60 mm × 500 mm elastomeric bearing pad (analysis 6); b) the block rail mounted on a 6 mm × 60 mm × 220 mm elastomeric bearing pad (analysis 7); c) the block rail mounted on two elastomeric bearing pads (analysis 8); d) the block rail with a 2 mm gap rigidly (analysis 9) or flexibly fixed (analysis 10) to the beam flange; e) the block rail with a 2 mm gap mounted on an elastomeric bearing pad (analysis 11)

In the case of the crane rail joint, two types were investigated, i.e., a continuous crane rail (Figs 3a–c and 4a–c) and a crane rail with a 2 mm gap (Figs 4d and 4e), to evaluate the impact of the crane rail joint type. The gap should not be larger than 2 mm [22], [23]. The crane rail joint may have different designs. Rykaluk et al. analysed three different types of crane rail joints, i.e., orthogonal contact, bevel contact, and stepped bevel contact [21]. The lowest

value of the local vertical compressive stress in the web was observed for the stepped bevel contact, while the highest value of the vertical compressive stress in the web was observed for the orthogonal contact. For this reason, the orthogonal contact, which provided for the highest stress value, was analysed in this paper.

In the case of the connection between the crane rail and the beam flange, three variants were studied. In the first variant, the crane rail was rigidly fixed to the beam flange (Figs 3a, 3b and 4d). In the second variant, the crane rail was flexibly fixed to the beam flange (Figs 3a, 3b and 4d), and in the third variant, the crane rail was mounted on a 6 mm elastomeric bearing pad (Figs 3c, 4a–c, 4e).

In the case of the elastomeric bearing pad, four variants were investigated. In the first one, a continuous 1-m-long elastomeric bearing pad was used (Figs 3c and 4e). In the second variant, a continuous 0.5-m-long elastomeric bearing pad was used (Fig. 4a). In the third variant, a continuous 0.22-m-long elastomeric bearing pad was used (Fig. 4b). In the fourth variant, two 0.5-m-long continuous elastomeric bearing pads were used with the joint located in the middle of the beam (Fig. 4c).

In the case of the rail wear, two variants were analysed. In the first variant the crane rail was not worn (Figs 3a, c and 4a–e). In the second variant the crane rail wear was taken into account by reducing the head of the rail by 25% (Fig. 3b).

### 3. Analytical approach

The local vertical compressive stress in the web  $\sigma_{\text{oz,Ed}}$  was calculated using Eq. (2). The results of these calculations are presented in Table 1.

Table 1. The local vertical compressive stress in the web  $\sigma_{\text{oz,Ed}}$  based on the standard [10]

No.	Crane rail	Connection	Elastomeric bearing pad	$\eta$ [%]	$t_r$ [mm]	$h_r$ [mm]	$b_{\text{eff}}$ [mm]	$I$ [cm <sup>4</sup> ]	$l_{\text{eff}}$ [cm]	$\sigma_{\text{oz,Ed}}$ [MPa]
1	<i>c</i>	<i>r</i>	–	0.0	60.0	60.0	132.0	252.5	22.1	56.5
2	<i>c</i>	<i>r</i>	–	25.0	45.0	45.0	117.0	122.3	17.4	71.9
3	<i>c</i>	<i>f</i>	–	0.0	60.0	60.0	132.0	108.0	16.8	74.5
4	<i>c</i>	<i>f</i>	–	25.0	45.0	45.0	117.0	45.6	12.7	98.8
5	<i>c</i>	<i>f</i>	6 × 60 × 1000	0.0	60.0	60.0	132.0	108.0	21.9	57.0
6	<i>c</i>	<i>f</i>	6 × 60 × 500	0.0	60.0	60.0	132.0	108.0	21.9	57.0
7	<i>c</i>	<i>f</i>	6 × 60 × 220	0.0	60.0	60.0	132.0	108.0	21.9	57.0
8	<i>c</i>	<i>f</i>	6 × 60 × 500 (× 2)	0.0	60.0	60.0	132.0	108.0	21.9	57.0
9	<i>g</i>	<i>r</i>	–	0.0	60.0	60.0	132.0	252.5	22.1	56.5
10	<i>g</i>	<i>f</i>	–	0.0	60.0	60.0	132.0	108.0	16.8	74.5
11	<i>g</i>	<i>f</i>	6 × 60 × 1000	0.0	60.0	60.0	132.0	108.0	21.9	57.0

*c* – continuous; *g* – with a 2 mm gap; *r* – rigid; *f* – flexible;  $\eta$  – rail head reduction;  $t_r$  – head height after reduction;  $h_r$  – rail height after reduction;  $b_{\text{eff}}$  – effective width of the top flange;  $I$  – second moment of area;  $l_{\text{eff}}$  – effective loaded length;  $\sigma_{\text{oz,Ed}}$  – local vertical compressive stress in the web

### 4. Numerical analyses

Non-linear finite element models of the crane runway beam were developed in the Abaqus program [24]. The calculations were performed using the Newton-Raphson method. Each numerical model consisted of a crane runway beam, a crane rail and two support plates. In some models a suitable resilient elastomeric bearing pad was applied under the crane

rail. Each model was 1.0 m long. The material behaviour of steel was modelled as bi-linear elastic-plastic with strain-hardening. The crane runway beam was made of S235 steel, and the crane rail and the support plates were made of S355 steel (Table 2). The material behaviour of the elastic underlay was modelled as elastic (Young's modulus  $E = 7.2$  MPa, Poisson's ratio  $\nu = 0.45$ ).

Table 2. Steel parameters [4]

Steel grade	Yield strength $f_y$ [MPa]	Ultimate tensile strength $f_u$ [MPa]	Young's modulus $E$ [GPa]	Poisson's ratio $\nu$ [-]
S235	235	360	210	0.3
S355	355	490	210	0.3

The wheel loading of 100 kN was introduced fully centrally. The vertical load was spread out over a 50-mm-wide area based on two European standards [25], [26]. In the case of the support plates and the runway beam contact, surface-to-surface contact was defined between the support plates and the beam flange. "Hard" contact was modelled in the normal direction and friction was modelled in the tangential direction. The friction coefficient between steel-steel elements was equal to 0.3. Depending on the model, three types of rail connection were modelled. In the case of the crane rail rigidly fixed to the beam flange, the rigid connection was modelled using the tie function. A surface-based tie constraint tied the crane rail and the beam flange together for the duration of the numerical simulations [24], [27]. In the case of the crane rail not rigidly fixed to the beam flange, surface-to-surface contact was defined between the crane rail and the beam flange. "Hard" contact was modelled in the normal direction and friction was modelled in the tangential direction. The friction coefficient between steel-steel elements was equal to 0.3. In the case of the crane rail mounted on a suitable resilient elastomeric bearing pad of 6 mm, surface-to-surface contact was defined between the crane rail and the bearing pad as well as between the bearing pad and the beam flange. "Hard" contact was modelled in the normal direction and friction was modelled in the tangential direction. The friction coefficient between steel-elastomeric bearing elements was equal to 0.3. The crane rail, the beam flanges and the elastomeric bearing pad were divided into eight-node cuboidal finite solid elements (C3D8R) and the crane runway beam stiffeners were divided into four-node shell elements (S4R). The maximum mesh size for these elements was 10 mm. The crane runway beam web was divided into four-node shell elements (S4R) of the maximum mesh size of 5 mm.

The chosen mesh size based on the analyses of the sensitivity of the numerical model to the mesh size presented in the literature [20, 21]. Chybiński et al. analysed two mesh sizes (5 mm and 10 mm) [20]. The local vertical compressive stress value in the web for the mesh size of 5 mm was 2.06% higher than for the mesh size of 10 mm. Rykaluk et al. presented that the difference in the local vertical compressive stress value in the web between the mesh size of 2 mm and 5 mm was only 0.53% [21]. They selected the mesh size of 5 mm for the numerical analyses. For this reason, in this paper, the mesh size of 5 mm was chosen for the web in the numerical simulations.

The shell web of the crane runway beam was connected with the solid flanges and the shell stiffeners using the tie function. Figure 5 presents the mesh and the boundary conditions used in the model (fixed displacements and rotations). The numerical analyses conducted in this study are presented in Table 3.

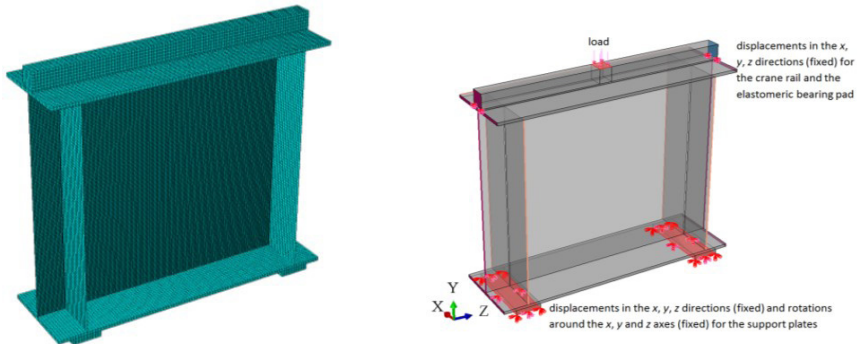


Fig. 5. The mesh and the boundary conditions used in the numerical model

Table 3. Numerical analyses

No.	Crane rail	Connection	Elastomeric bearing pad	$\eta$ [%]	$t_r$ [mm]	$h_r$ [mm]
1	<i>c</i>	<i>r</i>	–	0.0	60.0	60.0
2	<i>c</i>	<i>r</i>	–	25.0	45.0	45.0
3	<i>c</i>	<i>f</i>	–	0.0	60.0	60.0
4	<i>c</i>	<i>f</i>	–	25.0	45.0	45.0
5	<i>c</i>	<i>f</i>	6 × 60 × 1000	0.0	60.0	60.0
6	<i>c</i>	<i>f</i>	6 × 60 × 500	0.0	60.0	60.0
7	<i>c</i>	<i>f</i>	6 × 60 × 220	0.0	60.0	60.0
8	<i>c</i>	<i>f</i>	6 × 60 × 500 (× 2)	0.0	60.0	60.0
9	<i>g</i>	<i>r</i>	–	0.0	60.0	60.0
10	<i>g</i>	<i>f</i>	–	0.0	60.0	60.0
11	<i>g</i>	<i>f</i>	6 × 60 × 1000	0.0	60.0	60.0

*c* – continuous; *g* – with a 2 mm gap; *r* – rigid; *f* – flexible;  $\eta$  – rail head reduction;  $t_r$  – head height after reduction;  $h_r$  – rail height after reduction;  $b_{\text{eff}}$  – effective width of the top flange;  $I$  – second moment of area;  $l_{\text{eff}}$  – effective loaded length;  $\sigma_{\text{oz.Ed}}$  – local vertical compressive stress in the web

## 5. The results

The results of the analytical approach were compared with the results of the computer simulations in Table 4.

In the case of the continuous block rail rigidly fixed to the beam flange (analyses 1 and 2), satisfactory convergence of the local vertical compressive stress in the crane runway beam web was obtained. The stress values calculated using the analytical method in accordance with the standard [10] were only 3.7% (analysis 1) or (8.2%) (analysis 2) higher than the ones obtained from the numerical simulation. For the remaining analyses the stress obtained from the computer simulation was different from the one based on the analytical approach.

In the case of the continuous block rail flexibly fixed to the beam flange (analyses 3 and 4), the values of the local vertical compressive stress in the crane runway beam web calculated from the standard [10] were 21.9% (analysis 3) or 26.7% (analysis 4) higher than the ones obtained from the computer simulation. The numerical calculations underestimated the

maximum stress. This fact calls for further investigation and it should be verified in laboratory tests. It is worth emphasizing that the numerical calculations were only conducted for centric loading. What is more, the maximum stress in the numerical simulation increased significantly when the non-continuous block rail was used (analysis 10).

Table 4. The results of the analytical approach and computer simulations

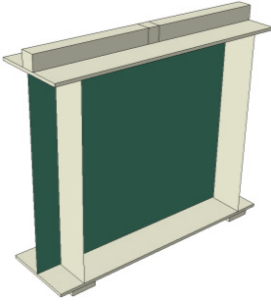
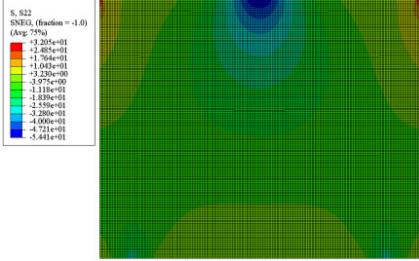
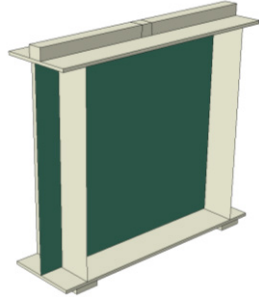
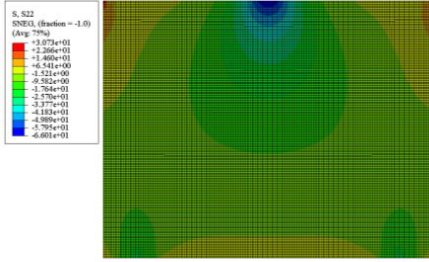
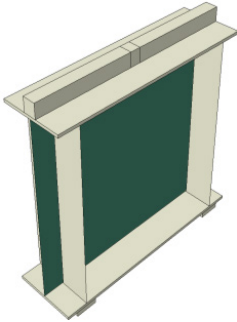
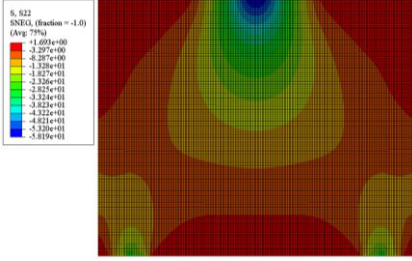
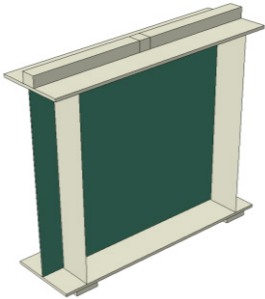
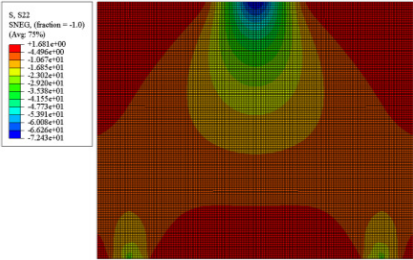
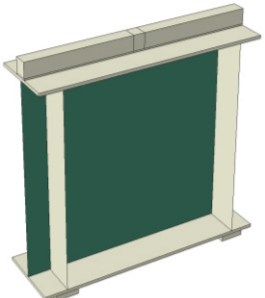
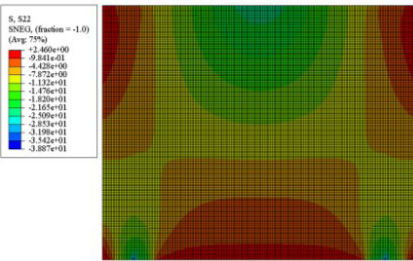
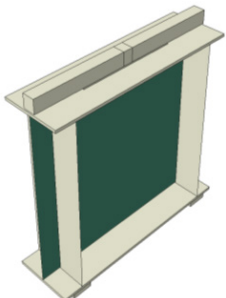
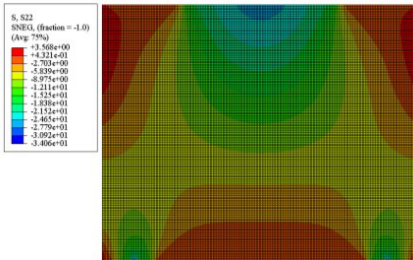
No.	Model	Stress distribution						
1		 <table border="1"> <thead> <tr> <th><math>\sigma_{oz,Ed,na}</math> [MPa]</th> <th><math>\sigma_{oz,Ed,s}</math> [MPa]</th> <th><math>\mu</math> [%]</th> </tr> </thead> <tbody> <tr> <td>54.4</td> <td>56.5</td> <td>-3.7</td> </tr> </tbody> </table>	$\sigma_{oz,Ed,na}$ [MPa]	$\sigma_{oz,Ed,s}$ [MPa]	$\mu$ [%]	54.4	56.5	-3.7
$\sigma_{oz,Ed,na}$ [MPa]	$\sigma_{oz,Ed,s}$ [MPa]	$\mu$ [%]						
54.4	56.5	-3.7						
2		 <table border="1"> <thead> <tr> <th><math>\sigma_{oz,Ed,na}</math> [MPa]</th> <th><math>\sigma_{oz,Ed,s}</math> [MPa]</th> <th><math>\mu</math> [%]</th> </tr> </thead> <tbody> <tr> <td>66.0</td> <td>71.9</td> <td>-8.2</td> </tr> </tbody> </table>	$\sigma_{oz,Ed,na}$ [MPa]	$\sigma_{oz,Ed,s}$ [MPa]	$\mu$ [%]	66.0	71.9	-8.2
$\sigma_{oz,Ed,na}$ [MPa]	$\sigma_{oz,Ed,s}$ [MPa]	$\mu$ [%]						
66.0	71.9	-8.2						
3		 <table border="1"> <thead> <tr> <th><math>\sigma_{oz,Ed,na}</math> [MPa]</th> <th><math>\sigma_{oz,Ed,s}</math> [MPa]</th> <th><math>\mu</math> [%]</th> </tr> </thead> <tbody> <tr> <td>58.2</td> <td>74.5</td> <td>-21.9</td> </tr> </tbody> </table>	$\sigma_{oz,Ed,na}$ [MPa]	$\sigma_{oz,Ed,s}$ [MPa]	$\mu$ [%]	58.2	74.5	-21.9
$\sigma_{oz,Ed,na}$ [MPa]	$\sigma_{oz,Ed,s}$ [MPa]	$\mu$ [%]						
58.2	74.5	-21.9						

Table 4. The results of the analytical approach and computer simulations, continued

No.	Model	Stress distribution			
4			$\sigma_{oz,Ed,na}$ [MPa]	$\sigma_{oz,Ed,s}$ [MPa]	$\mu$ [%]
			72.4	98.8	-26.7
5			$\sigma_{oz,Ed,na}$ [MPa]	$\sigma_{oz,Ed,s}$ [MPa]	$\mu$ [%]
			23.4	57.0	-58.9
6			$\sigma_{oz,Ed,na}$ [MPa]	$\sigma_{oz,Ed,s}$ [MPa]	$\mu$ [%]
			26.2	57.0	-54.0

In the case of the continuous block rail mounted on a 6 mm × 60 mm × 1000 mm elastomeric bearing pad (analysis 5), the local vertical compressive stress in the crane runway beam web calculated from the standard [10] was 58.9% higher than the one obtained from the computer simulation. A similar difference (43.3%) between the results of the analytical approach and the numerical simulation was obtained by Marcinczak [15]. In accordance with the standard [10], the effective length based on Eqs. (5) and (6) can be increased 1.3 times if an elastomeric bearing pad with a minimum thickness of 6 mm is used [28]. The maximum stress in the numerical simulation decreased 2.5 times when an underlay was used (compare analyses 3 and 5). This observation is optimistic and it calls for further investigation in

laboratory tests. Nevertheless, it should be noted that the numerical calculations were only conducted for centric loading. Furthermore, the maximum stress increased significantly in the numerical simulation when the non-continuous block rail was used (analysis 11) or when a shorter underlay was used (analysis 7). The non-continuous underlay investigated in analysis 8 did not have any impact on the web stress.

Table 4. The results of the analytical approach and computer simulations, continued

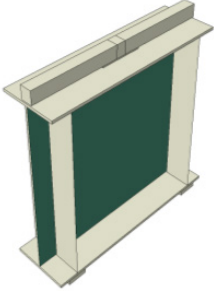
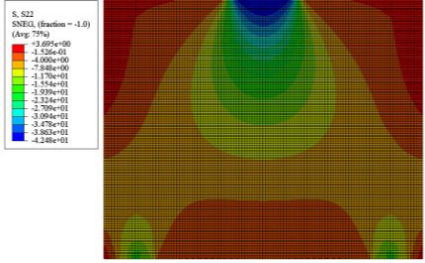
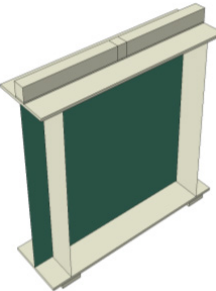
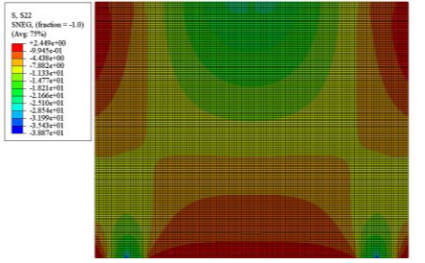
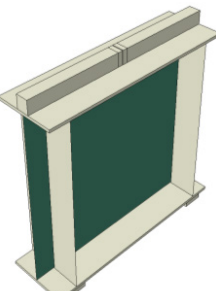
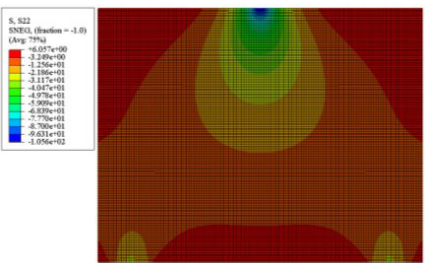
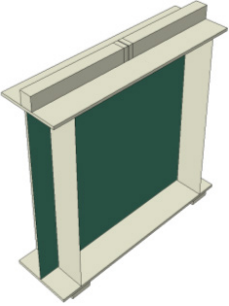
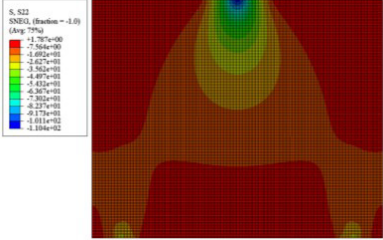
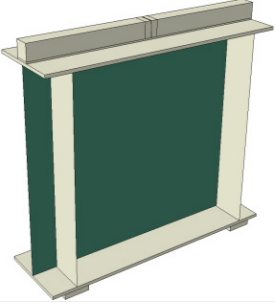
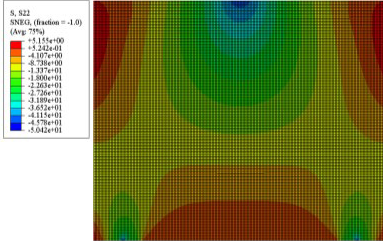
No.	Model	Stress distribution						
7		 <table border="1"> <thead> <tr> <th><math>\sigma_{oz,Ed,na}</math> [MPa]</th> <th><math>\sigma_{oz,Ed,s}</math> [MPa]</th> <th><math>\mu</math> [%]</th> </tr> </thead> <tbody> <tr> <td>42.5</td> <td>57.0</td> <td>-25.4</td> </tr> </tbody> </table>	$\sigma_{oz,Ed,na}$ [MPa]	$\sigma_{oz,Ed,s}$ [MPa]	$\mu$ [%]	42.5	57.0	-25.4
$\sigma_{oz,Ed,na}$ [MPa]	$\sigma_{oz,Ed,s}$ [MPa]	$\mu$ [%]						
42.5	57.0	-25.4						
8		 <table border="1"> <thead> <tr> <th><math>\sigma_{oz,Ed,na}</math> [MPa]</th> <th><math>\sigma_{oz,Ed,s}</math> [MPa]</th> <th><math>\mu</math> [%]</th> </tr> </thead> <tbody> <tr> <td>23.0</td> <td>57.0</td> <td>-59.6</td> </tr> </tbody> </table>	$\sigma_{oz,Ed,na}$ [MPa]	$\sigma_{oz,Ed,s}$ [MPa]	$\mu$ [%]	23.0	57.0	-59.6
$\sigma_{oz,Ed,na}$ [MPa]	$\sigma_{oz,Ed,s}$ [MPa]	$\mu$ [%]						
23.0	57.0	-59.6						
9		 <table border="1"> <thead> <tr> <th><math>\sigma_{oz,Ed,na}</math> [MPa]</th> <th><math>\sigma_{oz,Ed,s}</math> [MPa]</th> <th><math>\mu</math> [%]</th> </tr> </thead> <tbody> <tr> <td>105.4</td> <td>56.5</td> <td>86.5</td> </tr> </tbody> </table>	$\sigma_{oz,Ed,na}$ [MPa]	$\sigma_{oz,Ed,s}$ [MPa]	$\mu$ [%]	105.4	56.5	86.5
$\sigma_{oz,Ed,na}$ [MPa]	$\sigma_{oz,Ed,s}$ [MPa]	$\mu$ [%]						
105.4	56.5	86.5						

Table 4. The results of the analytical approach and computer simulations, continued

No.	Model	Stress distribution						
10		 <table border="1"> <thead> <tr> <th><math>\sigma_{oz,Ed,na}</math> [MPa]</th> <th><math>\sigma_{oz,Ed,s}</math> [MPa]</th> <th><math>\mu</math> [%]</th> </tr> </thead> <tbody> <tr> <td>110.4</td> <td>74.5</td> <td>48.2</td> </tr> </tbody> </table>	$\sigma_{oz,Ed,na}$ [MPa]	$\sigma_{oz,Ed,s}$ [MPa]	$\mu$ [%]	110.4	74.5	48.2
$\sigma_{oz,Ed,na}$ [MPa]	$\sigma_{oz,Ed,s}$ [MPa]	$\mu$ [%]						
110.4	74.5	48.2						
11		 <table border="1"> <thead> <tr> <th><math>\sigma_{oz,Ed,na}</math> [MPa]</th> <th><math>\sigma_{oz,Ed,s}</math> [MPa]</th> <th><math>\mu</math> [%]</th> </tr> </thead> <tbody> <tr> <td>42.7</td> <td>57.0</td> <td>-25.1</td> </tr> </tbody> </table>	$\sigma_{oz,Ed,na}$ [MPa]	$\sigma_{oz,Ed,s}$ [MPa]	$\mu$ [%]	42.7	57.0	-25.1
$\sigma_{oz,Ed,na}$ [MPa]	$\sigma_{oz,Ed,s}$ [MPa]	$\mu$ [%]						
42.7	57.0	-25.1						

$\sigma_{oz,Ed,na}$  – local vertical compressive stress in the crane runway beam web from numerical the analysis;  
 $\sigma_{oz,Ed,s}$  – local vertical compressive stress in the crane runway beam web based on the standard [10],  

$$\mu = \frac{\sigma_{oz,Ed,na} - \sigma_{oz,Ed,s}}{\sigma_{oz,Ed,s}} \cdot 10^2$$

## 6. Conclusions

In this paper, the authors focused on the local vertical compressive stress in the crane runway beam web. The stress was calculated using an analytical approach and numerical simulations. The connection between the block rail (60 mm × 60 mm) and the crane runway beam (IKS 800-6) was analysed in several variants. The study presented in this paper has certain limitations as within it, only the centric load position was investigated. What is more, no laboratory tests were performed on the crane runway beams. The results obtained in the numerical analyses were only compared with the results calculated using the analytical approach. It would be advisable to perform complementary laboratory tests to validate numerical models in the future. For this reason, the authors plan to conduct laboratory tests of crane runway beams.

The main conclusions, based on the calculations and the numerical analyses, are as follows:

- In the case of the continuous block rail rigidly fixed to the beam flange, the local vertical compressive stress in the crane runway beam web obtained from numerical simulations was in agreement with the results based on the standard [10].

- In the case of the continuous block rail flexibly fixed to the beam flange, the continuous block rail mounted on a 6 mm elastomeric bearing pad, and the non-continuous block rail, satisfactory convergence was not obtained. This fact calls for further investigation and it should be verified in laboratory tests.
- The crane rail joint had a significant impact on the web stress. For example, when the continuous crane rail was used (analysis 1) the stress was 1.94 times lower than when the crane rail with a 2 mm gap was used (analysis 9). In this paper the authors analysed the non-continuous crane rail with the worse orthogonal contact and the maximum possible gap (2 mm). The rules presented in the standard [10] do not take into account the crane rail joint. The standard underestimates the local value of the web stress. This fact is very important for designing crane runway beams, where crane rail joints are often used. The local web stress is added to the global stress due to bi-axial bending. A realistic evaluation of this local stress in the web is very important for verifying if the crane runway beams meet the ultimate limit state requirements of Eurocode 3 and for making accurate predictions of the fatigue life of the crane runway beams. For this reason, the standard [10] should be supplemented with the formulas for calculating the web stress also in the case of the non-continuous crane rails. What is more, a transverse stiffener should be used in the beam web under the rail joint, and stepped bevel contact should be used instead of orthogonal contact [21].
- The use of the a 6 mm elastomeric bearing pad provided for a significant reduction of the local stress value. For example, when comparing analyses 3 and 5 it can be seen that the maximum stress in the numerical simulation decreased 2.5 times when the underlay was used. However, the use of elastomeric bearing pads also has negative effects, as it provides for the increase of the deflection and tensile stress in crane rails [12], [14], [15].
- The length of the elastomeric bearing pad had an impact on the local stress value. This fact is of limited importance for designing crane runway beams, because in general continuous elastomeric bearing pads mounted under the rails are used.
- Last but not the least, the crane rail wear had a significant impact on the web stress. For this reason, a reduced rail head (by 25%) should be taken into account during the design process.

The results of this study indicate that further investigations, including laboratory tests, are necessary. Therefore, the authors plan to test real crane runway beams and study the effects of elastomeric bearing pads on the local vertical compressive stress in the crane runway beam web.

### Funding

This research was funded by the Polish Ministry of Science and Higher Education under the grant 0412/SBAD/0060.

### References

- [1] EN 1991-3, *Eurocode 1: Actions on structures, Part 3: Actions induced by cranes and machinery*, CEN, Brussels.
- [2] Kettler M., Kiem F. and Unterweger H., 2020. "Local stresses in retrofitted crane runway girders with boxed upper flange due to eccentric wheel loading", in *Structures*, vol. 25, (2020), pp. 646–656. <https://doi.org/10.1016/j.istruc.2020.03.024>
- [3] Żmuda J., *Konstrukcje wsporcze dźwignic*, Warszawa: Wydawnictwo Naukowe PWN, 2013.

- [4] EN 1993-1-1, *Eurocode 3: Design of steel structures, Part 1-1: General rules and rules for buildings*, CEN, Brussels.
- [5] Kurzawa Z., Rzeszut K. and Szumigala M., *Stalowe konstrukcje prętowe, cz. 3, Konstrukcje z lukami, elementy cienkościenne, pokrycia membranowe, elementy zespolone, dachy pierścieniowe i belki podsuwnicowe*, Poznań: Wydawnictwo Politechniki Poznańskiej, 2017.
- [6] Żmuda J. and Skowrońska J., “Wymiarowanie środników klasy 4. belek podsuwnicowych metodą naprężeń zredukowanych”, in *Inżynieria i Budownictwo*, 8, (2012), pp. 436–439.
- [7] Rykaluk K. and Hotała E., “Inicjowanie pęknięć zmęczeniowych w blachownicowych belkach podsuwnicowych”, in *Materiały Budowlane*, no. 5, (2014), pp. 84–86.
- [8] Kawecki P., Kawecki W. and Łaguna J., “Ocena zmęczenia stalowych belek podsuwnicowych na podstawie PN-EN 1993-6 i PN-EN 1993-1-9”, in *Inżynieria i Budownictwo*, no. 1, (2010), pp. 11–17.
- [9] Wichtowski B., 1997. “Analiza pęknięć zmęczeniowych w belkach podsuwnicowych w świetle badań”, in XVIII Konferencja Naukowo-Techniczna Awaryjne Budowlane, Szczecin-Międzyzdroje 19-22 maja 1997, 1997, pp. 507–514.
- [10] EN 1993-6, *Eurocode 3: Design of steel structures, Part 6: Crane supporting structures*, CEN, Brussels.
- [11] Kurzawa Z., “Wpływ tarcia powierzchniowego na cechy sprężyste podkładek pod szyny podsuwnicowe”, in *Zeszyty Naukowe Politechniki Poznańskiej. Budownictwo Lądowe*, vol. 39, (1995), pp. 95–101.
- [12] Biegus A., 2013. “Elastyczne połączenia konstrukcji wsporczej suwnic”, in *Inżynieria i Budownictwo*, no. 6, (2013), pp. 295–299.
- [13] Biegus A., 2014. “Podatne połączenia jezdni podsuwnicowych”, in *Builder*, vol. 198, no. 1, (2014), pp. 52–56.
- [14] Maas G., “Investigations concerning craneway girders”, in *Iron and Steel Engineer*, vol. 3, (1972), pp. 49–58.
- [15] Marcinczak K., 2017. “Redukcja naprężeń w środniku belki podsuwnicowej”, in *Builder*, vol. 242, no. 9, (2017), pp. 60–63.
- [16] Kurzawa Z., Chybiński M. and Polus Ł., “Wzrost lokalnych pionowych naprężeń ściskających w środniku belki podsuwnicowej ze względu na zużycie szyny”, in *Inżynieria i Budownictwo*, no. 11-12, (2022), pp. 553–557.
- [17] Jankowiak W., *Wybrane konstrukcje stalowe*, Poznań: Wydawnictwo Politechniki Poznańskiej, 1992.
- [18] Górski S., Kurzawa Z. and Murkowski W., *Przykłady obliczeń konstrukcji stalowych, cz. 2, Hale przemysłowe*, Poznań: Wydawnictwo Politechniki Poznańskiej, 1987.
- [19] Giżejowski M., Ziółko J., Barcewicz W., Irek K., Kawecki J., Kozłowski A., Kubiszyn W., Matuszkiewicz M., Ślęczka L., Pałkowski S., Rykaluk K., Włodarczyk W. and Żmuda J., *Projektowanie wybranych stalowych konstrukcji specjalnych z przykładami obliczeń*, Warszawa: Wydawnictwo Arkady, 2022.
- [20] Chybiński M., Kurzawa Z. and Polus Ł., “Wpływ rodzaju szyny na wartość lokalnych pionowych naprężeń ściskających w środniku belki podsuwnicowej”, in *Przegląd Budowlany*, no. 11-12, (2022), pp. 35–41.
- [21] Rykaluk K., Marcinczak K. and Rowiński S., “Fatigue hazards in welded plate crane runway girders – Locations, causes and calculations”, in *Archives of Civil and Mechanical Engineering*, vol. 18, (2018), pp. 69–82. 10.1016/j.acme.2017.05.003
- [22] Kurzawa Z., *Stalowe konstrukcje prętowe, cz. 1, Hale przemysłowe oraz obiekty użyteczności publicznej*, Poznań: Wydawnictwo Politechniki Poznańskiej, 2012.

- 
- [23] Matysiak A. and Grochowska E., *Konstrukcje stalowe. Belki podsuwnicowe. Estakady, cz. 1, Belki podsuwnicowe*, Zielona Góra: Oficyna Wydawnicza Uniwersytetu Zielonogórskiego, 2016.
- [24] Abaqus 6.13 Documentation, Abaqus Analysis Users Guide, Abaqus Theory Guide.
- [25] DIN 4132, *Kranbahnen; Stahltragwerke, Grundsätze für Berechnung, bauliche Durchbildung und Ausführung*, Berlin, 1981.
- [26] EN 13001-3-1:2013, *Cranes – General Design – Part 3-1: Limit States and Proof Competence of Steel Structure*, CEN, Brussels.
- [27] Dębski H., Ponieważ G., Różyło P. and Wójcik A., *Podstawy metody elementów skończonych – przykłady obliczeń numerycznych w programie Abaqus®*, Lublin: Politechnika Lubelska, 2015.
- [28] Kettler M., Kamleitner A., Novak F., Mandl A. and Unterweger H., “Local stresses in webs of crane runway girders: Tests and numerical calculations”, in *Journal of Constructional Steel Research*, vol 139, (2017), pp. 188–201. 10.1016/j.jcsr.2017.09.016